Biochimica et Biophysica Acta 1861 (2017) 58–67

Contents lists available at ScienceDirect

Biochimica et Biophysica Acta

journal homepage: www.elsevier.com/locate/bbagen

Quantitative analysis of the role of fiber length on phagocytosis and inflammatory response by alveolar macrophages

Trudy Padmore [a], Carahline Stark [a], Leonid A. Turkevich [b], Julie A. Champion [a,*]

[a] Chemical & Biomolecular Engineering, Georgia Institute of Technology, United States
[b] CEMB/DART/NIOSH/CDC, United States

ARTICLE INFO

Article history:
Received 7 April 2016
Received in revised form 16 July 2016
Accepted 20 September 2016
Available online 23 October 2016

Keywords:
Macrophage
Glass fibers
Length
Frustrated phagocytosis
TNF-α: Tumor necrosis factor-α

ABSTRACT

Background: In the lung, macrophages attempt to engulf inhaled high aspect ratio pathogenic materials, secreting inflammatory molecules in the process. The inability of macrophages to remove these materials leads to chronic inflammation and disease. How the biophysical and biochemical mechanisms of these effects are influenced by fiber length remains undetermined. This study evaluates the role of fiber length on phagocytosis and molecular inflammatory responses to non-cytotoxic fibers, enabling development of quantitative length-based models.
Methods: Murine alveolar macrophages were exposed to short and long populations of JM-100 glass fibers, produced by successive sedimentation and repeated crushing, respectively. Interactions between fibers and macrophages were observed using time-lapse video microscopy, and quantified by flow cytometry. Inflammatory biomolecules (TNF-α, IL-1α, COX-2, PGE_2) were measured.
Results: Uptake of short fibers occurred more readily than for long, but long fibers were more potent stimulators of inflammatory molecules. Stimulation resulted in dose-dependent secretion of inflammatory biomolecules but no cytotoxicity or strong ROS production. Linear cytokine dose-response curves evaluated with length-dependent potency models, using measured fiber length distributions, resulted in identification of critical fiber lengths that cause frustrated phagocytosis and increased inflammatory biomolecule production.
Conclusion: Short fibers played a minor role in the inflammatory response compared to long fibers. The critical lengths at which frustrated phagocytosis occurs can be quantified by fitting dose-response curves to fiber distribution data.
General significance: The single physical parameter of length can be used to directly assess the contributions of length against other physicochemical fiber properties to disease endpoints.

1. Introduction

Phagocytosis by macrophages is critical in the degradation and clearance of pathogenic materials in the body [1]. High aspect ratio materials such as asbestos fibers or carbon nanotubes can be cleared by phagocytosis or persist and induce frustrated phagocytic interactions leading to chronic inflammation, oxidative stress, direct cell injury, and chromosomal abnormalities [2–5]. This evasion can lead to diseases such as fibrosis, asbestosis, lung cancer, mesothelioma for asbestos-like materials, and carbon nanotubes have recently been shown to induce asbestos-like chronic inflammation. In this work we define frustrated phagocytosis as the failure to engulf after attaching, spreading and manipulation of fibers by macrophages. The extent to which high aspect ratio materials evade clearance is strongly length-dependent, both *in vivo* and *in vitro*[6–17]. However, there is no consensus about a critical length beyond which materials persist, as these studies are confounded by other material physicochemical properties such as diameter and surface chemistry, or by cell type and location within the body.

For asbestos specifically, comparative study of length-based contributions between different types remains challenging since they possess different physicochemical properties and lead to varied disease endpoints and health outcomes, ranging from cancerous lesions to genotoxicity [18–21]. *In vivo* study of the role of fiber length on disease endpoints is further complicated by other length-dependent processes, which can obscure any correlation of residual fibers with the disease endpoint. *In situ* fiber breakage reduces the population of long fibers and increases the population of short fibers [22]. *In situ* dissolution reduces fiber diameter, which may then lead to additional breakage [23, 24]. Phagocytosis removes shorter fibers, changing the length distribution over time. Translocation reduces the fiber population at the deposition site and, together with all clearance mechanisms, may have an efficiency that depends on fiber length [25]. It is thus difficult to

* Corresponding author.
E-mail address: julie.champion@chbe.gatech.edu (J.A. Champion).

http://dx.doi.org/10.1016/j.bbagen.2016.09.031
0304-4165/

associate unambiguously fibers recovered in pathology with those that have induced disease. In *in vitro* experiments, after an induction time, macrophages will successfully engulf short fibers, and we lose the information of whether the short-fiber/cell interaction differs from the long-fiber/cell interaction. Therefore, we need to monitor cell-fiber interactions on short timescales following initial contact. An *in vitro* model that quantitatively captures all length-based contributions to the cellular response is critical to understanding pathogenic mechanisms.

A challenge in studying the effect of fiber properties in biological systems is the difficulty in obtaining fiber samples with well-controlled physical properties. The Baron dielectrophoretic classifier enabled earlier studies with length-separated glass fibers [15,16], while the use of JM-100 model glass fibers decouples fiber length from surface chemistry. Blake et al. [15] and Ye et al. [16] revealed a length-dependent cytotoxicity and induction of inflammatory cytokines after exposure of alveolar macrophages to glass fibers of varied lengths *in vitro*. However, while the Baron classifier can prepare short fibers with a narrow distribution of lengths, the long fibers are inherently broad in their length distribution. Without characterization of long fiber length distributions, it is not possible to attribute a critical fiber length to the cellular responses reported.

Here we present a quantitative assessment of phagocytic and inflammatory responses of MH-S murine alveolar macrophages to long and short populations of JM-100 glass fibers with well-characterized fiber distributions. Parameterization of the length distributions enabled the development of models that propose critical lengths for varied phagocytic interactions between fibers and cells. These length-dependent interactions were captured by time-lapse microscopy and flow cytometry. Production of inflammatory biomolecules, tumor necrosis factor α (TNF-α), Interleukin-1 α (IL-1α), cyclooxygenase-2 (COX-2), and prostaglandin E2 (PGE_2), was quantified after macrophage exposure to short and long glass fiber populations. These pathological hallmarks are evidence of macrophage activation and fiber-induced inflammatory signaling [17]. We used the dose-response curves of the directly-stimulated cytokines (TNF-α, IL-1α) to identify critical fiber lengths that increase inflammatory biomolecule production in macrophages during frustrated phagocytosis of long fibers.

2. Materials and Methods

2.1. Fiber sample preparation

Fibers were prepared from a Pall glass fiber depth filter sheet, type AE binder free (Pall Life Sciences, Ann Arbor, MI, available as SKC no. 225-7-07, SKC Inc., Eighty Four, PA). This media consisted of entangled uncoated borosilicate glass fibers (of nominal diameters 0.1 μm < d < 10 μm), designed to retain 1-μm particles on liquid filtration. Batches of 24 sheets were cut out to fit into a 1¼″ die cavity and crushed with a lab press for 60 s. Short fibers were obtained by crushing at 10 tons and re-crushed at 15 tons, while long fibers were crushed at 2 tons. Each batch yields ~1.3 g of fiber [26].

Individual fibers were liberated from the residual fibrous mat after crushing through suspension in 500 mL of DI water and sonication (Fisher Scientific Sonic Dismembrator Model 500 with ½″ horn), at 50% amplitude (*i.e.* tip amplitude ~76 μm), for 30 min (1 s on, 1 s off). This procedure was followed to prepare the stock suspension of short fibers (no sedimentation step). The long fiber samples were allowed to gravitationally settle for 20 min, with the resulting supernatant decanted. The sediment was re-suspended in 500 mL and sonicated as described above. This sonication, settling, decanting, re-suspension procedure was iterated 10 times; the 10th sediment constituted the long fiber sample. All samples were prepared for diameter measurement by vacuum filtering 1 mL of a 1000:1 dilution through a 0.8 μm nitrocellulose filter (Millipore AAWP 02500); deposition is nominally ~1 $\mu g/cm^2$.

2.2. Fiber length measurement

All fiber samples were subjected to a final filtration through a 35 μm mesh to separate entangled fibers before length measurement and exposure to macrophages. Fibers were imaged (see Time-Lapse Video Microscopy section) on an incubation stage of an Axio Observer Z1 inverted light microscope (Carl Zeiss Microscopy, LLC, Thornwood, NY) and observed using differential interference contrast at 100× magnification. This imaging differs from the typical phase contrast microscopy analysis of fibers collected on acetone cleared MCE filters [27,28].

The length of the fibers was measured, using the line tool from Motic Images Plus 2.0 ML (Motic Group, Richmond, BC, Canada); faint fibers were identified with the aid of the magnification tool at 200% magnification. Only fibers entirely contained within the field of view were included for length measurement; this restriction actually biases the measured length distribution against the longer fibers, but since the dimensions of the field of view (220 μm × 170 μm) are quite large compared to almost all of the measured fibers, this distortion was neglected (Turkevich, unpublished). At this magnification, 1 μm represents the image resolution limit.

2.3. Fiber diameter measurement

Fibers were imaged with scanning electron microscopy (SEM) to analyze fiber diameter. The nitrocellulose filters were mounted on 25 mm planchettes or stubs, using colloidal graphite adhesive, and were sputter coated with gold, to prevent charging by the electron beam. The samples were analyzed using a Hitachi S3000N scanning electron microscope. Secondary electron images were obtained at an accelerating voltage of 25 keV. Images were taken at 800× and 4000×. The length and diameter of the fibers were again measured using the line tool from Motic Images Plus 2.0 ML. At 800×, fiber diameter quantitation was not possible below 0.25 μm; at 4000×, fiber diameter quantitation was not possible below 0.15 μm.

2.4. Fiber count

Serial dilutions of suspended fibers were counted using a haemocytometer mounted on a light microscope at 40× magnification; fiber counts were accepted when the difference in count among serial dilutions was <5%. Short fiber counts were verified by an Accuri C6 flow cytometer (Becton Dickinson). Dose-response experiments were reported as a function of optically detected (40× mag) fibers/cell.

2.5. Fiber labeling with fluorescent probe

Approximately 1.5 mg of glass fibers were suspended in 1 mL of 1 M KOH by sonication (pulse mode; 4 s on, 2 s off; 30% amplitude; 2 min total process time) and incubated for one hour. Fibers were washed with 1 mL deionized water (18.3 MΩ·cm at 25 °C) followed by a wash with 1 mL ethanol. Washes consisted of centrifuging the fibers at 125 ×*g* for 5 min, 2400 ×*g* for 10 min, and 21,000 ×*g* for 1 min. To maximize fiber retention while minimizing breakage of fibers, the fiber pellet was retained after each centrifugation step and only the supernatant was centrifuged in the next step. Fibers were dried in an oven at 37 °C for 1.5 h. Fibers were then incubated for 2 min in a solution of 1 mL toluene and 33 μL 3-mercaptopropyl trimethoxysilane, washed with excess toluene to remove unconjugated silane, and suspended in 1 mL of 20 mM N-[Tris(hydroxymethyl)methyl]-2-aminoethanesulfonic (TES) sodium salt buffer solution. 15 μl of 20 mM of 5-iodoacetamidofluorescein (5-IAF) in dimethyl formamide (DMF) was added. The reaction was allowed to proceed in the dark for 2 h at 4 °C under constant stirring. Fibers were washed twice in deionized water by centrifugation at 125 ×*g* for 5 min, 2400 ×*g* for 10 min, and 21,000 ×*g* for 1 min to remove unreacted reagents before exposure to cells.

2.6. Alveolar macrophages

Immortalized MH-S murine alveolar macrophages (ATCC-CRL2019) were used as model macrophages. They were cultured in RPMI media supplemented with 10% fetal bovine serum, 1% penicillin-streptomycin, and 50 μM beta-mercaptoethanol at 37 °C in a humidified atmosphere containing 5% CO_2. MH-S macrophages possess increased homogeneity of response in comparison to their highly heterogeneous primary macrophage counterparts. The cytokine response is known to differ among primary macrophage cell type. Immortalized cells are less responsive to cytotoxic stimuli and are thus ideal as model macrophages for dose-response testing of stimuli that are typically cytotoxic at high doses.

2.7. Time-lapse video microscopy

Macrophages, 3.2×10^4 cells/cm^2 in culture media, were seeded in a glass bottom dish and placed in an incubation stage on an Axio Observer. Z1 inverted microscope (Carl Zeiss, Inc.) and observed using differential interference contrast at 100× magnification. Cells were allowed to attach for 1 h before short or long fibers were added to the center of the dish. Images of fiber-cell interactions were captured every 2 min by a Zeiss AxioCam camera for 24 h. Images were collected and compiled into videos using AxioVision software and manually analyzed for cell-fiber interactions. Successful phagocytic internalization was characterized by membrane ruffling at the site of attachment, blurring of the crisp boundary of the membrane, and subsequent reformation of the membrane boundary after internalization. In addition, a fiber was only classified as internalized if it remained within the cell membrane boundary for the remaining observation period. Fibers with incomplete internalization and/or attachment were seen to cross the cell membrane of mobile cells.

2.8. Quantification of fiber internalization and attachment

Macrophages were plated at 5.3×10^4 cell/cm^2 in a 48-well plate and incubated for 24 h. Cell culture media was replaced with identical media containing fibers at various concentrations for 24 h. Short fibers were incubated at concentrations of 5, 10, and 20 fibers/cell, while long fibers were incubated at concentrations of 5, 7.5, and 10 fibers/cell. Cells were harvested by scraping, centrifuged at 125 × *g* for 5 min followed by suspension in 200 μl PBS. Short fiber internalization and attachment events were distinguished by the use of trypan blue, which quenches fluorescence of externally bound fibers but not internalized fibers. Half of each cell sample was mixed with equal volumes of either PBS (unquenched) or trypan blue (quenched), and filtered with 35 μm mesh. Cell fluorescence was measured with an Accuri C6 flow cytometer. The cell populations were gated to exclude free fibers not associated with cells. Cells were identified as associated with fibers if their fluorescence was greater than cell autofluorescence measured in the absence of fibers for both the trypan blue quenched and PBS unquenched conditions.

Images of long fiber interactions with macrophages were captured after 24 h by a Zeiss AxioCam camera (Phase contrast 40 X magnification). Internalization and attachment interactions were quantified after visual inspection of randomly selected images of each fiber/cell concentration. The process was repeated three times and the average count reported. A total of 700 fiber-cell interactions were recorded.

2.9. Inflammatory biomolecule and cytotoxicity measurements

Macrophages were seeded in 6-well plates (5.3×10^4 cells/cm^2) for COX-2 and PGE_2 measurements, and in 96-well plates (1.6×10^5 cells/cm^2) for TNF-α and IL-1α measurements, for 24 h. Cell culture media was replaced with identical media containing fibers at concentrations of 5–15 long fibers/cell and 10–150 short fibers/cell. Bacterial lipopolysaccharide (1 μg/mL LPS) was used as an inflammatory stimuli positive control. After 24 h of cell-fiber incubation, supernatants were harvested for TNF-α, IL-1α, and PGE_2 and interrogated by ELISA following R&D Systems (Minneapolis, MN) instructions. Supernatants were also used to determine cytotoxicity by detection of lactate dehydrogenase (LDH) with a colorimetric assay based on the reduction of pyruvate from Thermo Scientific (Waltham, MA). Cell lysates were collected and used for COX-2 ELISA (R&D Systems) following the manufacturer's instructions. All cell fiber conditions were repeated in triplicate, and results were validated with three separate preparations of short and long fibers.

2.10. Reactive oxygen species (ROS) production

Macrophages were seeded in 48-well plates (5.3×10^4 cell/cm^2) for 24 h prior to pretreatment with 10 μM dose of the non-fluorescent, membrane-permeable dye 6-carboxy-2′,7′-dichlorodihydrofluorescein diacetate (carboxy-H2DCFDA, ThermoScientific, Grand Island, NY) at 37 °C for 20 min. Esterases in the cells convert carboxy-H2DCFDA to the charged form to increase intracellular retention. Cells were then washed with PBS before treatment with short and long fibers for 24 h as detailed in the inflammatory biomolecule and cytotoxicity section above. Carboxy-H2DCFDA is chemically reduced by intracellular reactive oxygen species (ROS) to become fluorescent. Cell fluorescence was detected using a fluorescent plate reader (Biotek, Winooski, VT).

2.11. Statistical analysis

Data are presented as mean ± standard deviation of the mean of representative experiments. Group means were compared using Student *t*-test or one-way analysis of variance. $P < 0.05$ was considered statistically significant.

2.12. Length-derived parameters and model fitting

In our fitting of these models, the length distribution of the fibers is represented by log-normal distribution,

$$f(\ln(L)) = \left(2\pi\sigma^2\right)^{-\frac{1}{2}} * \exp\left[\frac{-(\ln(L)-\mu)^2}{2\sigma^2}\right], \quad (1)$$

with parameters;

Short fibers: $\mu = 1.946 = \ln(7.0)$ and $\sigma = 0.971$
Long fibers: $\mu = 3.671 = \ln(39.3)$ and $\sigma = 0.739$

Similar determinations could have been made directly using the length histograms; however, the shot noise inherent in the finite binning of the histograms introduces additional interpolation uncertainty.

Since the fiber populations differ only in their length distributions, for the case of direct stimulation, the ratio of the slopes of the dose-response curves depend on a potency function, p(L), averaged over the length distribution: <p(L)>. In each of the three models, the function p(L) is defined and <p(L)> is calculated.

2.12.1. Model 1 - length cut-off, L_c

Model assumption - Fibers shorter than L_c elicited no cytokine response, while all fibers longer than L_c contributed equally to the cytokine response. The potency function $p(L)$ is given by:

$$p(L) = \begin{cases} 0, & L<L_c \\ p_0, & L>L_c \end{cases} \quad (2)$$

The model attributes fiber potency to the number of fibers not internalized by macrophages, generating an average potency

$$<p> = p_0\,[\,1 - cum(L_c)], \quad (3)$$

where *cum*(*L*) is the cumulant of the fiber length distribution. For a log-normal fiber distribution (Eq. (1)), the average potency (Eq. (3)) becomes.

$$<p> = \left(\frac{p_0}{\sigma}\right) erfc\left[\frac{\ln(L_c) - \mu}{\sqrt{2\sigma}}\right] \quad (4)$$

where erfc(x) is the complementary error function.

2.12.2. Model 2 - power-law potency

Model assumption - Fiber potency varies as a power law of the length, weighting very long fibers as more 'problematic' for macrophages.

$$p(L) \sim L^{\alpha} \quad (5)$$

For a log-normal length distribution (Eq. (1)), the average potency becomes

$$<L^{\alpha}> = \exp\left(\alpha\mu + \alpha^2\frac{\sigma^2}{2}\right) \quad (6)$$

2.12.3. Model 3 - power-law potency with a cut-off

Model assumption - Fibers shorter than a cut-off, L_c, do not elicit a cytokine response from macrophages, while fibers longer than this cut-off elicited a response that scales as a power of the length.

$$p(L) = \begin{cases} 0, & L<L_c \\ p_0 L^{\alpha}, & L>L_c \end{cases} \quad (7)$$

In this model, fibers that are internalized by macrophages do not contribute to the cytokine response, and, of the *non-internalized fibers*, the longer ones are more potent. For a log-normal distribution (Eq. (1)), the average potency becomes

$$<p> = \left(\frac{p_0}{\sigma}\right) * exp\left(\alpha\mu + \frac{\alpha^2\sigma^2}{2}\right) * erfc\left[\frac{\ln(L_c) - \mu - \alpha\sigma^2}{\sqrt{2\sigma}}\right] \quad (8)$$

where, again, erfc(x) is the complementary error function.

3. Results

3.1. Fiber length and diameter distribution

Subsequent to their separation into "short" and "long" populations by high pressure crushing, and low pressure crushing followed by repeated sedimentation, respectively, the diameter and length of fiber samples were measured. Fig. 1 shows the length distributions of the two populations. The fiber length distributions were confirmed to be log-normal (Fig. 1 inset) where mean length, μ, was 7.0 μm and 39.3 μm for short and long fibers, respectively. Electron micrographs of typical short and long fibers are shown in Supplementary Fig. S1. Fiber diameter is centered around d ~ 0.8 μm (Supplementary Fig. S2) and is uncorrelated with fiber length (Supplementary Fig. S3).

3.2. Fiber-cell interactions

The immortalized murine MH-S alveolar macrophage cell line was used as a model to examine the role of glass fiber length in uptake, cytotoxicity, and inflammatory response. Real-time images of fiber-cell interactions were captured using time-lapse microscopy. A total of twenty-five fiber-cell interaction events, in which fibers either attached to or were internalized by macrophages, were recorded. Fig. 2 provides snapshots showing representative interactions – internalization of a short fiber and frustrated phagocytosis of a long fiber. Cell membrane ruffling can be seen at the site of attachment to the short fiber with subsequent blurring of the crisp boundary of the membrane. A membrane boundary reformed after the fiber is completely engulfed by the cell with the fiber remaining in the same focal plan and relative position within the cell (Supplementary Movie 1). The cell interacting with the long fiber can be seen to attach with a pseudopod-like projection, pull the fiber toward it, and spread along a small region of the fiber. It is evident that the cell can exhibit significant force on the fiber as it flips the fiber vertically 180° (Supplementary Movie 2). The scenario in which the macrophage is 'speared' on the fiber was never observed, nor was any cell blebbing upon fiber-cell interactions. Internalization events were fewer for long fibers in comparison to short; 25% of cell binding events with short fibers resulted in phagocytic internalization, while only 12% of long fiber binding events were internalization events. Only frustrated phagocytosis was observed to occur for fibers >16 μm.

For high throughput quantification of fiber-cell interactions, fibers were covalently conjugated with fluorescent probe IAF (5-Iodoacetamidofluorescein) for detection by flow cytometry (Supplementary Fig. S4). Cell fluorescence was measured in the absence or presence of extracellular fluorescence quenching agent trypan blue to measure the combination of attached and internalized fibers or only internalized fibers, respectively. This measurement counts relative populations of cells but does not yield information on, the number of fibers associated with a cell. Therefore, internalization refers to the complete phagocytosis of *at least one* labeled fiber, and attachment refers to attachment of *at least one* labeled fiber. The cells exhibited a dose-dependent increase in total short fiber interactions, but the *relative* fraction of

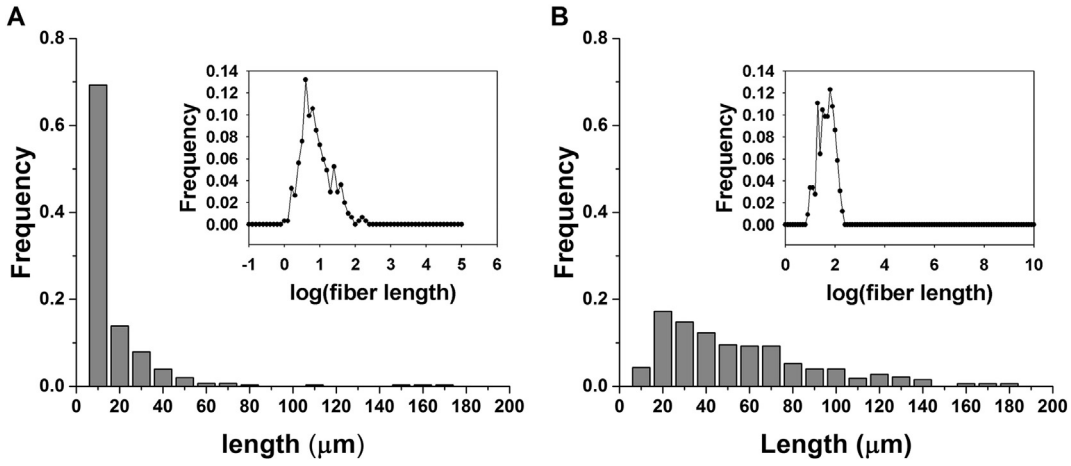

Fig. 1. Fiber length distribution. Representative histograms of the length distributions of (A) short and (B) long fibers. Both populations exhibit a log-normal distribution for fiber lengths (inset).

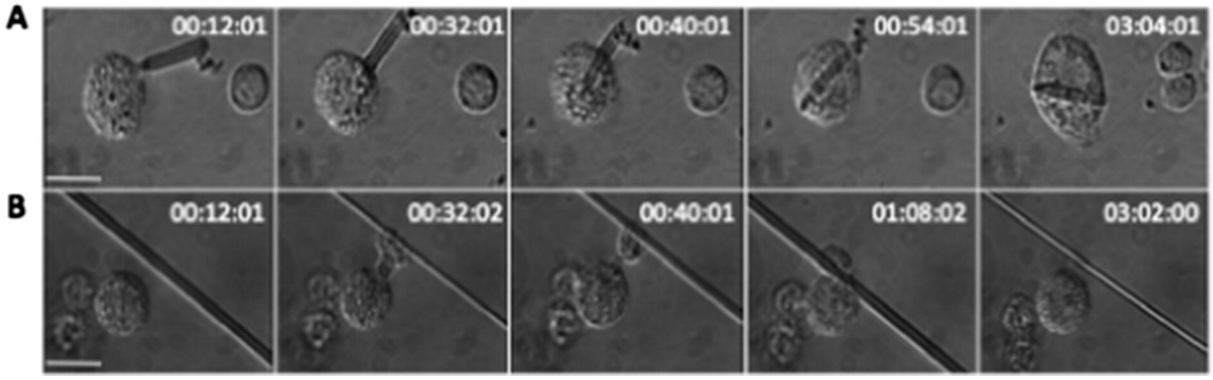

Fig. 2. Time-lapse video microscopy frames of macrophage-fiber binding events. (A) A short fiber being internalized by a macrophage. (B) A macrophage attaching to and pulling a long fiber toward itself without internalization. Scale bar: 20 μm, Time: 0–3 h.

cells with internalized fibers compared to attached was independent of concentration (Fig. 3). Flow cytometry was not feasible for long fibers due to the similarity in lengths of the long fibers and the core diameter of the flow cytometer fluidics components. However, quantification of long fiber-cell interactions at 24 h post-incubation by optical observation at 40× magnification revealed a similar independence of internalization with increased long fiber dose (Supplementary Fig. S5).

3.3. Fiber cytotoxicity

Macrophages were exposed to short and long fibers for 24 h, and released cytosolic lactate dehydrogenase (LDH) was measured from culture supernatants as a measure of cytotoxicity. The fiber-exposed macrophages exhibited no detectable LDH cytotoxicity, *i.e.* the normalized optical absorption fell below the limit of detection range (LOD = 12.5 ± 3.5%) of the media blanks. Fiber concentrations ranging from 0 to 15 long fibers/cell, and 0–150 short fibers/cell exhibited no cytotoxicity (Fig. 4).

3.4. Fiber induced ROS activity

Cell permeating fluorescent probes such as DCDHF has been used to measure intracellular ROS activity in fiber-stimulated macrophages [29, 30]. DCDHF is used to measure the cumulative ROS [31] response after 24 h of fiber stimulation to macrophages. Activity of the carboxy-H2DCFDA, a DCDHF derivative, probe was confirmed by LPS stimulation of macrophages (positive control, supplementary data Fig. S7). Cumulative intracellular reactive oxygen species (ROS) production in response to either long or short fibers is weak. Individual experiments all exhibited ROS signals below the LOD. Attempts to pool the data, using, as a standard, the ROS signal generated from cells stimulated by LPS (at 1 μg/mL) resulted in low R^2 values indicative of minimal statistical correlation due to this standard signal variance. The pooled data suggest: i) ROS production in response to the glass fibers is detectable, and ii) increased ROS production following exposure to long (*vs.* short) fibers. However, we caution that the ROS signals are all weak, and the above suggestions are not statistically significant. A detailed statistical analysis of the ROS measurements is provided in the Supplementary Data.

3.5. Fiber induced inflammatory molecule production

Four inflammatory-related molecules were measured by ELISA following 24 h of exposure to fibers. TNF-α cytokine secretion exhibited a linear dose-response on a per fiber basis (Fig. 5). The signal is strong (much larger than the LOD = 16 pg/mL and LOQ = 44 pg/mL). Long fibers produced greater inflammatory biomolecule secretion than short fibers. The ratio of the TNF-α dose response slopes of long to short fibers was $m_L/m_S = 11.1$, with a 95% confidence interval of $9.1 < m_L/m_S < 13.3$.

Cytokine IL-1α was secreted in very low quantities, but above the limit of detection (LOD = 1.4 pg/mL, LOQ = 6.5 pg/mL). Again, both long and short fibers exhibited linear dose responses (Fig. 6). The ratio of long and short fibers slopes of the IL-1α dose-response curves $m_L/m_S = 11.3$, with a 95% confidence interval of $8.1 < m_L/m_S < 15.7$.

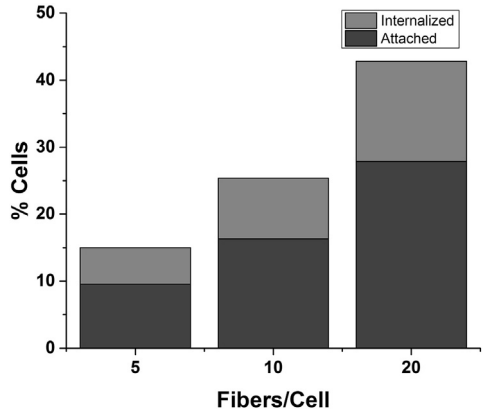

Fig. 3. Fiber-cell interactions with increasing short fiber dosage. Fiber-cell interactions quantified by flow cytometry reveal a dose-dependent increase in all interactions for short fibers. The relative percentage of cells with internalized interactions compared to total interactions was relatively unchanged for all fiber doses, with 36.4%, 35.7%, and 34.9% for short fiber doses 5, 10, and 20 respectively. A total of 10,000 cells were counted including cells with no associated fibers.

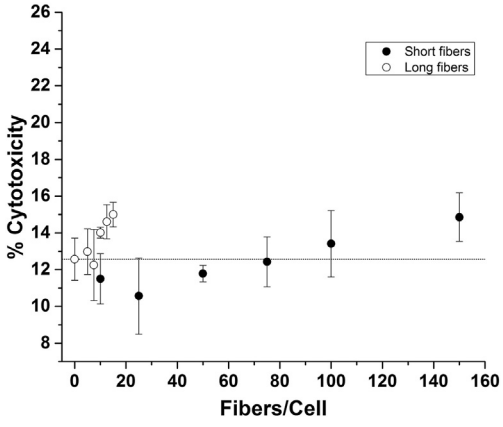

Fig. 4. Cytotoxicity of macrophages exposed to short and long fibers. The percentage cytotoxicity was measured as the quantity of LDH released from fiber-damaged cells relative to a lysed cell control. Normal cell turnover corresponds to 0 fibers/cell and is noted by a dashed line (–). On average fiber cytotoxicity was not significant for both short and long fiber populations as compared to the media blank with the exception of the maximum long fiber dose, 15 long fibers/cell. *$p < 0.05$.

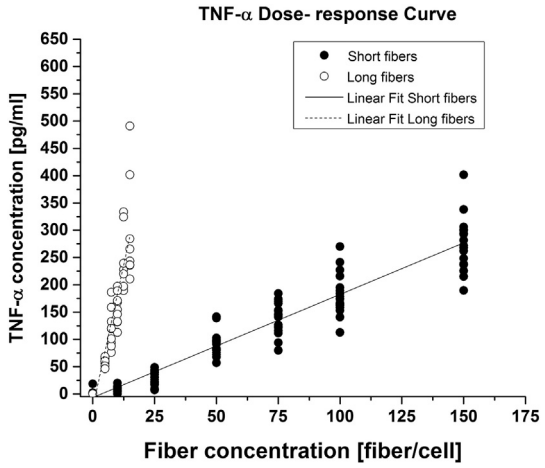

Fig. 5. TNF-α dose-response curves. TNF-α secretion showed a linear dose response for short and long glass fibers. Data shown was collected for three (3) independent experiments.

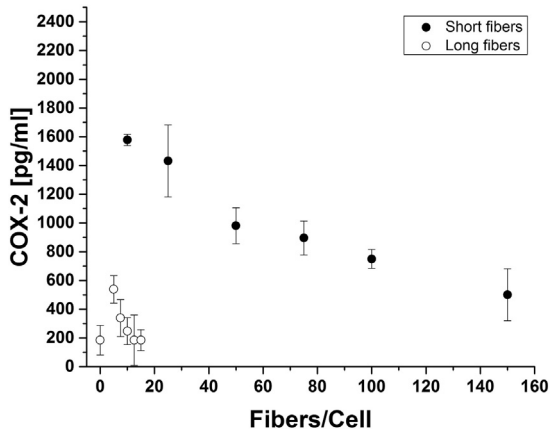

Fig. 7. COX-2 Enzyme Production. COX-2 production decreased with increasing fiber dose -short fiber stimulation resulted in significantly high expression of COX-2 while long fibers were generally comparable to no fiber stimulation.

Cyclooxygenase-2 (COX-2) production by fiber-treated macrophages depended inversely on fiber dose (Fig. 7). The variation of the fiber-stimulated COX-2 production is complicated by the fact that it depends both directly on the stimulating fibers but also indirectly on the cytokine TNF-α, whose production is also stimulated by the fibers [32]. We noted that COX-2 production varies inversely with TNF-α expression (Supplementary Fig. S5).

Prostaglandin E2 (PGE_2) is a secreted downstream metabolite of the COX enzymatic pathway. PGE_2 secretion was greater for long fibers than short fibers (Fig. 8). The measured signal from PGE_2 secretion was low, but there was a weak observed linear dose-response for long fibers. PGE_2 production for short fibers was neither statistically significant, *i.e.* most signals were below the limit of detection (LOD = 55 pg/mL), nor dose-dependent.

4. Discussion

This work uses model glass fibers with measured length distributions and model alveolar macrophages to assess fiber length effects on phagocytosis and associated inflammatory biomolecule production, and to develop the quantitative model described below. The use of glass fibers eliminates contributions of surface chemistry and diameter from those of fiber length. Macrophages are highly heterogeneous cells, and immortalized mouse MH-S alveolar macrophages were chosen as model macrophages because of their increased homogeneity in response to particles of various shapes and sizes [33,34]. Although cytokine response varies across macrophage source, macrophage dose-response is investigated here, and analysis of the change in response is used to build our models. While cytotoxicity by glass fibers is less pronounced for immortalized cell lines [16] than for primary cell line [7, 15], the trends of cytokine response for short and long fibers are the same. Moreover, MH-S macrophages have been shown to function similarly to primary cells for phagocytic interactions and IL-1α cytokine response [35,36].

Stanton performed an exhaustive study across various asbestos types and hypothesized that asbestos fiber dimension and durability, rather than other physicochemical properties, were responsible for fiber-related biological effects *in vivo*[10]. The latency of asbestos-associated pulmonary diseases, as well as the established link between chronic inflammation and cancer [20,21], supports this theory of chronic inflammation resulting from biopersistence as the prevailing cause of disease pathology [6,37–40]. *In vivo* and *in vitro* studies examining the role of fiber length on biopersistence also support this theory. Goodglick et al. showed that both short and long asbestos fibers were cytotoxic *in vitro*, while short fibers were cytotoxic when clearance was prevented *in vivo*[8]. In threshold length studies using silver nanowires Schinwald and colleagues identified *in vivo* threshold lengths of L > 4 μm, and 11–14 μm for fiber-induced pleura [9] and pulmonary [41] inflammation respectively. McDonald and colleagues described long fibers (>10 μm) as having the greater pathogenic risk than short fibers (<6 μm) *in vivo*[42]. However, direct comparison among different forms of asbestos remains challenging due to fiber heterogeneity. Comparative length dependent

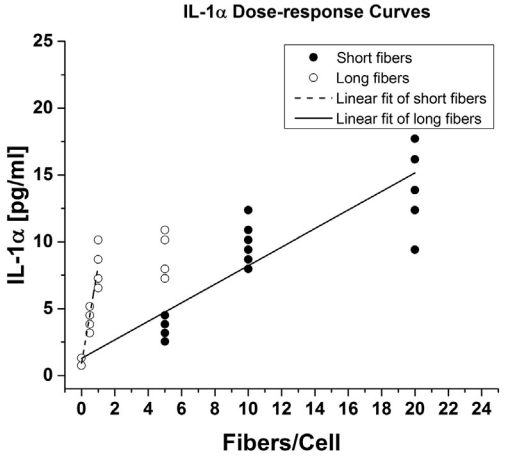

Fig. 6. IL-1α dose-response curves. IL-1α secretion showed a linear dose response for short and long fibers. Data shown was collected from three (3) independent experiments.

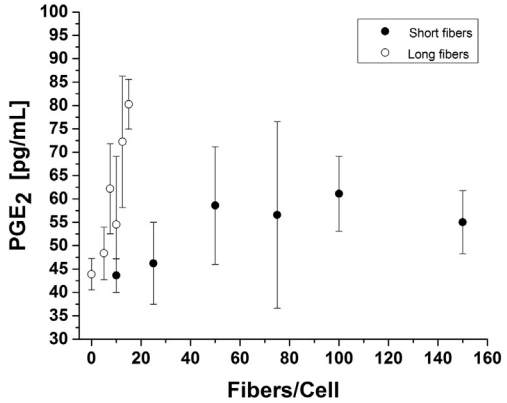

Fig. 8. Prostaglandin E2, PGE_2, production 24 h post-incubation. Short fiber response was independent of fiber concentration. Long fibers showed weak dose dependence in comparison to 0 fibers/cell control.

studies, using actual asbestos fibers, have neither been able to characterize fibers within narrow length-classified size ranges, nor separate other confounding fiber parameters such as diameter, chemistry, and surface properties. Indeed, recent studies of asbestos-like high aspect ratio nanomaterials, of which carbon nanotubes are a subset, have shown that these fibers elicit an inflammatory response due also to surface chemistry-related reactivity and thus are unable to isolate length-based contributions to the biological effects. This highlighted the need for model materials in which pathogenic parameters can be isolated and accurately characterized in order to determine single-parameter contributions to disease endpoints. To this end, *in vitro* studies using glass fibers identified length dependence to the inflammatory response and speculated that increased inflammatory response was due to frustrated phagocytosis of longer fibers. Blake et al. observed a length-dependent cytotoxicity and production of reactive oxygen species after exposure of alveolar macrophages to glass fibers of varied lengths [15]. Ye et al. showed that long fibers (17 μm) were significantly more potent than short fibers (7 μm) in inducing inflammatory NF-kB activation and TNF-α production [16]. Zeidler-Erdely et al. also found that glass fiber >17 μm were cytotoxic to human primary macrophages [7]. Here we are able to quantify phagocytic interactions and corresponding molecular responses from accurately characterized glass fibers to develop a model that can be used to evaluate the isolated contributions of fiber length to macrophage interactions.

Real-time imaging of interactions between macrophages and fibers revealed internalization, attachment and frustrated phagocytosis outcomes within short and long samples, suggesting weighted contributions of these processes to the overall inflammatory response. We saw that the fraction of internalized long fibers was less than that of short fibers, with long fibers undergoing frustrated phagocytosis due to the inability of the cell to effectively phagocytize fibers. No spearing or damage to the cell membrane was observed. Since, there is ample microscopy evidence for such processes in the literature [6,11], they are either rare, dependent on macrophage type, fiber diameter and type [43] or occurs on time-scales longer than the 24 h of our time-lapse experiments. Our observation of macrophage biochemical response to fibers on the short timescale implicates a mechanism other than spearing responsible for increased inflammatory response. Comparison of the average contact surface areas, which scales with fiber length at constant diameter, of long and short internalized fibers, revealed no relationship between quantities of fibers internalized and their average fiber lengths. Thus, internalization does not scale solely with average fiber length, suggesting that other more complex length models are possible. The quantity of internalized short fibers was limited only by fiber concentration, as flow cytometry data showed increased internalization with increased short fiber concentration.

Similar to the cytotoxic findings of Ye et al. with immortalized peritoneal macrophages [16], we found no relationship between fiber length and cytotoxicity. Neither increases in attachment nor internalization had adverse cytotoxic effects. Likewise, cumulative intracellular ROS production by fiber-stimulated macrophages is weak, with, perhaps, an enhancement in ROS production by macrophages stimulated by the long fibers (Supplementary Fig. S7). Reactive oxygen species (ROS) are a complex array of highly reactive molecules including H2O2, HOCl, *OH, *O, and superoxide anion compounds. In phagocytes oxidative stress responses at the plasma membrane in response to extracellular pathogenic material [44], and metal ions [2,45] can lead to the generation of extracellular ROS compounds. Generation of ROS by NADPH oxidase also occurs in intracellular compartments such as phagosomal membranes and mitochondria.

In fiber induced diseases ROS plays a pivotal role through fiber-mediated respiratory bursts [46], and frustrated phagocytosis [47]. ROS also plays a role both in cell signaling [48], activation of cytokine transcription [49], and oxidative stress-mediated cytotoxicity [50]. Increasing levels of intracellular ROS is indicative of cell toxicity [51]. The low intracellular ROS produced by glass fiber stimulation is expected, given the observed lack of cytotoxicity. The low level of ROS produced did not permit significant length-based conclusion, as demonstrated by Brown et al. in the study of morphological dependence on phagocytosis of carbon nanotubes [52].

Cytokines TNF-α and IL-1α are secreted in response to inflammatory stimuli. TNF-α has been identified as a critical mediator of fiber-related pathogenicity [16], while pro-inflammatory cytokine IL-1α works in concert with TNF-α and is induced following NF-κB activation [53]. IL-1α secretion has also been reported upon exposure to carbon nanotubes [54,55]. Additionally, IL-1α, along with IL-1β, is indicative of inflammasome activation [56,57]. Studies have shown that the inflammasome is activated upon stimulation by asbestos fibers, carbon nanotubes, and nanoparticles [47,58,59] with reports of dose-dependent secretion of IL-1α [58,60]. Similar to Palomaki and colleagues, glass-fiber stimulation of IL-1α secretion was both dose- and length-dependent [58].

NF-κB has been shown to a have a length-dependent activation by glass fibers [16]. Comparison of the slopes of the dose-response curves for TNF-α and IL-1α showed a greater response to long fibers than to short fibers (Figs. 5, 6). TNF-α cytokine secretion did not scale with the average fiber length. We would expect the ratio of the slopes of short and long cytokine response curves to be the same as the ratio of the short and long average fiber lengths (7 μm/39.3 μm) if cytokine secretion scaled only with fiber length. Additionally, short fibers produced a weaker inflammatory response per fiber. By extension, complete phagocytosis of fibers has minimal contribution to the inflammatory response. This agrees with contributions of 'frustrated' phagocytic interaction or incomplete internalization of longer fibers to the inflammatory condition [61].

We assessed the ability of the fibers to stimulate pathogenic markers, cyclooxygenase-2 (COX-2) and its downstream metabolite, prostaglandin E2 (PGE_2). COX-2 is known to modulate carcinogenesis. It is induced by oxidative stress and inflammatory cytokine secretion, which are key mechanisms of asbestos fiber responses in cells [62]. Fiber-treated macrophages demonstrated an inverse relationship between TNF-α and COX-2 at 24 h post-incubation (Supplementary Fig. S6). Literature supports that this modulatory action may be NF-κB dependent. Not only is NF-κB known to up-regulate COX-2, but COX-2 activity in turn affects NF-κB [63,64]. Past studies of inflammatory regulation reveal a temporally destabilizing effect of TNF-α on COX-2 mRNA [32]. Our COX-2 results supports this proposed feedback action of COX-2, since at short time scales production of PGE_2 is weak but shows concomitant increases with TNF-α.

We have attempted to rationalize the cytokine data, which demonstrates the increased relative potency of long over short fibers with three simple models—that may be treated as a phenomenological parameterization of the data. These models were fitted only to TNF-α and IL-1α, since they are directly stimulated by the fibers; by contrast, COX-2 and PGE_2 depend both directly on the stimulating fiber and also indirectly, through the cytokines generated by the macrophages responding to fibers. The two fiber populations differed only in their distribution of lengths, not diameters or chemistry. Thus the ratio of the slopes of the dose-response curves can only depend on some potency function, $p(L)$, averaged over the length distribution: $\langle p(L) \rangle$.

In the first model, a simple length cut-off, L_c, is posited so that fibers shorter than L_c elicit no cytokine response, and that all fibers longer than L_c contribute equally to the cytokine response; the potency function $p(L)$ is given by:

$$p(L) = \begin{cases} 0, & L<L_c \\ p_0, & L>L_c \end{cases} \quad (2)$$

Using the fitted parameters for short and long fiber distributions, we obtain $L_c = 27.0$ μm, with a 95% confidence interval 22.9 μm < L_c < 31.4 μm for TNF-α, and $L_c = 27.4$ μm, with a 95% confidence interval 20.8 μm < L_c < 36.0 μm from the IL-1α response. It is

remarkable that these two cytokines, TNF-α and IL-1α, yield similar relative potencies of the long and short fibers. Furthermore, the cut-off length is quite reasonable when compared to the size of macrophages. Typical rodent alveolar macrophages are ~13 μm in suspension [65]. However, plated macrophages spread to larger diameters, 20.7 ± 8.8 μm in this work, and are the appropriate comparison since all experiments were performed on plated cells.

In the second model, long fibers are modeled as being more potent than short through a power law:

$$p(L) \sim L^{\alpha} \tag{5}$$

There is no cut-off length in this model. Using the fitted parameters for short and long fiber distributions we obtain $\alpha = 1.75$, with a 95% confidence interval $1.56 < \alpha < 1.93$ for TNF-α, and $\alpha = 1.76$, with a 95% confidence interval $1.46 < \alpha < 2.11$ from the IL-1α response. Most physical quantities relevant to fiber -cell interactions, such as average fiber length, average volume, mass, average surface area, all scale as $<L>$ (*i.e.* $\alpha = 1$) and thus $\alpha > 1$ is unreasonable. Our results thus argue for either a stronger length variation of potency (stronger than a power law, or for an additional reduced potency of the short fibers *e.g.* through a length cut-off, L_c).

In a third two-parameter model, fibers longer than a cut-off, L_c, elicit a response, scaling as a power of the length, that is, longer non-internalized fibers, are weighted more; the appropriate potency function is

$$p(L) = \begin{cases} 0, & L<L_c \\ p_0 L^{\alpha}, & L>L_c \end{cases} \tag{7}$$

If we force $\alpha = 1$, we obtain $L_c = 12.1$ μm, with a 95% confidence interval $7.7\ \mu m < L_c < 16.3\ \mu m$ for TNF-α, and $L_c = 12.5$ μm, with a 95% confidence interval $4.9\ \mu m < L_c < 20.6\ \mu m$ from the IL-1α response. Again, the cut-off lengths determined by these independent cytokine measurements are very similar.

With a cut-off, if there is no additional length dependence of the potency ($\alpha = 0$), we obtain $L_c \sim 27$ μm, comparable to the plated macrophage size. If, with a cut-off, the potency of the non-phagocytosed fibers depends on the standard physical parameters ($\alpha = 1$), we obtain $L_c \sim 12$ μm, shorter than the macrophage size, but not unreasonable. Frustrated phagocytosis was observed by time-lapse microscopy for length, $L > 16$ μm, which is consistent with the cut-offs obtained from the first and third models; we have no independent criteria to prefer the first model over the third model. We note that, $\alpha = 1.75$ from a simple power law potency (second model) seems unreasonable.

Schinwald and colleagues reported a critical length range of 5 μm for onset of frustrated phagocytosis in a primary alveolar *in vitro* migration assay [41]. However, considering the contribution of fiber length distribution, and *in vitro* assay type we cautiously report that the authors' threshold length is within the range of our third model predictions. Schinwald et al. proposes that mechanical obstruction of long bulky fibers may have led to decreasing mobility with increasing fiber length. We have also observed that multiple cells will simultaneously attempt to engulf the same longer fiber which may lead to low cell mobility, as seen by Schinwald et al. Given our frequency of fiber length, with 40% of short glass fibers and 95% of our long fibers being greater than the silver nanowire lengths examined a migration assay would not have been feasible for direct comparison of threshold lengths.

Our models suggest that fiber-cell interaction differs above and below a critical fiber length; fibers with lengths $L < L_c$ contribute minimally to inflammatory biomolecule production, while the majority of biomolecule production is due to frustrated phagocytosis of fibers of length $L > L_c$. L_c should be viewed as a statistical parameter, as variations in macrophage cell and fiber-cell orientation will influence the outcome of individual fiber-cell interactions. The output of the length-based models may change with fiber and cell type. The degree, to which this occurs, along with *in vivo* validation of *in vitro* findings, will be the focus of our future work. By establishing glass fiber length-based models as a control, the question of the extent to which length potentiates the adverse effects of other physicochemical parameters of asbestos fibers can be answered. Importantly, independent of the detailed modeling, these studies have shown that, even for very short induction times (~24 h), there is significant length dependence to the response of macrophage cells phagocytic interactions with fibers.

5. Conclusion

Our results show that the single physical parameter of length plays an important role in fiber-induced macrophage inflammatory responses. Pro-inflammatory cytokines, TNF-α and IL-1α, were shown to increase in both a dose and length dependent manner. Short fibers were more readily internalized and played a minor role in inflammatory biomolecule production compared to long fibers on a per-fiber basis. The MH-S cell line showed no dose toxicity allowing us to reproducibly evaluate dose-response up to two orders of magnitude. Importantly, for our stimulating material, characterization revealed no correlation between fiber diameter distribution and length distribution, so we are able to isolate the effect of fiber length on the macrophage response. This distinguishes our study from previous work on length dependence of frustrated phagocytosis and inflammatory responses. Here we show a universal dose-response approach to determining critical length and present two possible models that describes phagocytic interactions: a critical length based model in which the potency of longer fibers are equally weighted, and a two-parameter power law and potency model in which the weighting is skewed toward longer fibers. Each model produces reasonable critical lengths for frustrated phagocytosis: 27 μm and 12 μm respectively.

Supplementary data are available online. Word (.docx) and Movie (.MPEG) files. Supplementary data associated with this article can be found in the online version, at http://dx.doi.org/10.1016/j.bbagen.2016.09.031.

Funding

This work was supported by the National Institute of Occupational Safety and Health (NIOSH).

Disclaimer

The findings and conclusions in this paper are those of the authors and do not necessarily represent the views of the National Institute for Occupational Safety and Health. Mention of product or company name does not constitute endorsement by the Centers for Disease Control and Prevention.

Transparency document

The Transparency document associated with this article can be found, in online version.

Acknowledgements

We thank J.E. Fernback (NIOSH) for electron microscopy, G. Deye (NIOSH) and NIOSH co-op students E. Ashley, J. Schirmer (U. Cincinnati), E. Clark (Northern Kentucky U.), C. Lauber (Texas Tech. U.) for assistance with sample preparation (fiber crushing and sedimentation), optical microscopy and fiber counting. We thank the following colleagues from NIOSH: the late P. Baron for introducing us to this problem; V. Castranova (also at West Virginia U.) for helpful discussions; M. Waters, S. Shulman, P. Shaw, A. Feng for helpful statistical discussions; M. Waters, K. Ashley, D. Farwick for their careful reading of the manuscript; D. Weissman, A. Munson, P. Middendorf for ongoing support of this line of research.

References

[1] A. Aderem, D. Underhill, Mechanisms of phagocytosis in macrophages, Annu. Rev. Immunol. 17 (1999) 593–623.
[2] A. Shukla, M. Gulumian, T.K. Hei, D. Kamp, Q. Rahman, B.T. Mossman, Multiple roles of oxidants in the pathogenesis of asbestos-induced diseases, Free Radic. Biol. Med. 34 (2003) 1117–1129.
[3] S. Toyokuni, Role of iron in carcinogenesis: cancer as a ferrotoxic disease, Cancer Sci. 100 (2009) 9–16.
[4] N.S. Wang, M.C. Jaurand, L. Magne, L. Kheuang, M.C. Pinchon, J. Bignon, The interactions between asbestos fibers and metaphase chromosomes of rat pleural mesothelial cells in culture. A scanning and transmission electron microscopic study, Am. J. Pathol. 126 (1987) 343–349.
[5] J.G. Ault, R.W. Cole, C.G. Jensen, L.C.W. Jensen, L.A. Bachert, C.L. Reider, Behavior of crocidolite asbestos during mitosis in living vertebrate lung epithelial cells, Cancer Res. 55 (1995) 792–798.
[6] K. Donaldson, F.A. Murphy, R. Duffin, C.A. Poland, Asbestos, carbon nanotubes and the pleural mesothelium: a review of the hypothesis regarding the role of long fibre retention in the parietal pleura, inflammation and mesothelioma, Part. Fibre Toxicol. 7 (2010) 5.
[7] P.C. Zeidler-Erdely, W.J. Calhoun, B.T. Ameredes, M.P. Clark, G.J. Deye, P. Baron, W. Jones, T. Blake, V. Castranova, In vitro cytotoxicity of Manville code 100 glass fibers: effect of fiber length on human alveolar macrophages, Part. Fibre Toxicol. 3 (2006) 5.
[8] L.A. Goodglick, A.B. Kane, Cytotoxicity of long and short crocidolite asbestos fibers in vitro and in vivo, Cancer Res. 50 (1990) 5153–5163.
[9] A. Schinwald, F.A. Murphy, A. Prina-Mello, C.A. Poland, F. Byrne, D. Movia, J.R. Glass, J.C. Dickerson, D.A. Schultz, C.E. Jeffree, W. MacNee, K. Donaldson, The threshold length for fiber-induced acute pleural inflammation: shedding light on the early events in asbestos-induced mesothelioma, Toxicol. Sci. 128 (2012) 461–470.
[10] M.F. Stanton, M.W. Layard, Carcinogenicity of natural and man-made fibers, Adv. Clin. Oncol. 1 (1978) 181–187.
[11] F.A. Murphy, A. Schinwald, C.A. Poland, K. Donaldson, The mechanism of pleural inflammation by long carbon nanotubes: interaction of long fibres with macrophages stimulates them to amplify pro-inflammatory responses in mesothelial cells, Part. Fibre Toxicol. 9 (2012) 8.
[12] B.G. Miller, A. Searl, J.M.G. Davis, K. Donaldson, R.T. Cullen, R.E. Bolton, D. Buchanan, C.A. Soutar, Influence of fibre length, dissolution and biopersistence on the production of mesothelioma in the rat peritoneal cavity, Ann. Occup. Hyg. 43 (1999) 155–166.
[13] K. Donaldson, G.M. Brown, D.M. Brown, R.E. Bolton, J.M. Davis, Inflammation generating potential of long and short fibre amosite asbestos samples, Br. J. Ind. Med. 46 (1989) 271–276.
[14] J.M.G. Davis, J. Addison, R.E. Bolton, K. Donaldson, A.D. Jones, T. Smith, The pathogenicity of long versus short fibre samples of amosite asbestos administered to rats by inhalation and intraperitoneal injection, Br. J. Exp. Pathol. 67 (1986) 415–430.
[15] T. Blake, V. Castranova, D. Schwegler-Berry, P. Baron, G.J. Deye, C. Li, W. Jones, Effect of fiber length on glass microfiber cytotoxicity, J. Toxic. Environ. Health A 54 (1998) 243–259.
[16] J. Ye, X. Shi, W. Jones, Y. Rojanasakul, N. Cheng, D. Schwegler-Berry, P. Baron, G.J. Deye, C. Li, V. Castranova, Critical role of glass fiber length in TNF-alpha production and transcription factor activation in macrophages, Am. J. Phys. 276 (1999) 426–434.
[17] K. Donaldson, B.G. Miller, E. Sara, J. Slight, R.C. Brown, Asbestos fibre length-dependent detachment injury to alveolar epithelial cells in vitro: role of a fibronectin-binding receptor, Int. J. Exp. Pathol. 74 (1993) 243–250.
[18] B.T. Mossman, M. Lippmann, T.W. Hesterberg, K.T. Kelsey, A. Barchowsky, J.C. Bonner, Pulmonary endpoints (lung carcinomas and asbestosis) following inhalation exposure to asbestos, J. Toxicol. Environ. Health B Crit. Rev. 14 (2011) 76–121.
[19] K. Hansen, B.T. Mossman, Generation of superoxide (O2-) from alveolar macrophages exposed to asbestiform and nonfibrous particles, Cancer Res. 47 (1987) 1681–1686.
[20] H. Yang, M. Bocchetta, B. Kroczynska, A.G. Elmishad, Y. Chen, Z. Liu, C. Bubici, B.T. Mossman, H.I. Pass, J.R. Testa, G. Franzoso, M. Carbone, TNF-alpha inhibits asbestos-induced cytotoxicity via a NF-kappaB-dependent pathway, a possible mechanism for asbestos-induced oncogenesis, Proc. Natl. Acad. Sci. U. S. A. 103 (2006) 10397–10402.
[21] M. Philip, D.A. Rowley, H. Schreiber, Inflammation as a tumor promoter in cancer induction, Semin. Cancer Biol. 14 (2004) 433–439.
[22] A. Searl, D. Buchanan, R.T. Cullen, A.D. Jones, B.G. Miller, C.A. Soutar, Biopersistence and durability of nine mineral fibre types in rat lungs over 12 months, Ann. Occup. Hyg. 43 (1999) 143–153.
[23] J.M.G. Davis, The role of clearance and dissolution in determining the durability or biopersistence of mineral fibers, Environ. Health Perspect. 102 (1994) 113–117.
[24] A. Morgan, A. Holmes, W. Davison, Clearance of sized glass fibres from the rat lung and their solubility in vivo, Ann. Occup. Hyg. 25 (1982) 317–331.
[25] M. Lippmann, D.B. Yeates, R.E. Albert, Deposition, retention, and clearance of inhaled particles, Br. J. Ind. Med. 37 (1980) 337–362.
[26] K.J. Cho, L. Turkevich, M. Miller, R. McKay, S.A. Grinshpun, K. Ha, T. Reponen, Penetration of fiber versus spherical particles through filter media and faceseal leakage of N95 filtering facepiece respirators with cyclic flow, J. Occup. Environ. Hyg. 10 (2013) 109–115.
[27] B.K. Ku, G. Deye, L.A. Turkevich, Characterization of a vortex shaking method for aerosolizing fibers, Aerosol Sci. Technol. 47 (2014) 1293–1301.
[28] B. Ku, G. Deye, L. Turkevich, Efficacy of screens in removing long fibers from an aerosol stream–sample preparation technique for toxicology studies, Inhal. Toxicol. 26 (2014) 70–83.
[29] S.K. Sohaebuddin, P.T. Thevenot, D. Baker, J.W. Eaton, L. Tang, Nanomaterial cytotoxicity is composition, size, and cell type dependent, Part. Fibre Toxicol. 7 (2010) 22.
[30] A. Xu, H. Zhou, D.Z. Yu, T.K. Hei, Mechanisms of the genotoxicity of crocidolite asbestos in mammalian cells: implication from mutation patterns induced by reactive oxygen species, Environ. Health Perspect. 110 (2002) 1003–1008.
[31] L. Müller, M. Riediker, P. Wick, M. Mohr, P. Gehr, B. Rothen-Rutishauser, Oxidative stress and inflammation response after nanoparticle exposure: differences between human lung cell monocultures and an advanced three-dimensional model of the human epithelial airways, J. R. Soc. Interface 7 (2010) 27–40.
[32] Z.-F. Huang, J.B. Massey, D.P. Via, Differential regulation of cyclooxygenase-2 (COX-2) mRNA stability by interleukin-1β (IL-1β) and tumor necrosis factor-α (TNF-α) in human in vitro differentiated macrophages, Biochem. Pharmacol. 59 (2000) 187–194.
[33] J.A. Champion, S. Mitragotri, Role of target geometry in phagocytosis, Proc. Natl. Acad. Sci. U. S. A. 103 (2006) 4930–4934.
[34] J.A. Champion, A. Walker, S. Mitragotri, Role of particle size in phagocytosis of polymeric microspheres, Pharm. Res. 25 (2008) 1815–1821.
[35] I.N. Mbawuike, H.B. Herscowitz, MH-S, a murine alveolar macrophage cell line: morphological, cytochemical, and functional characteristics, J. Leukoc. Biol. 46 (1989) 119–127.
[36] K. Matsunaga, T.W. Klein, H. Friedman, Y. Yamamoto, Alveolar macrophage cell line MH-S is valuable as an in vitro model for legionella pneumophila infection, Am. J. Respir. Cell Mol. Biol. 24 (2001) 326–331.
[37] J. Bignon, R. Saracci, J.C. Touray, Introduction: INSERM-IARC-CNRS workshop on biopersistence of respirable synthetic fibers and minerals, Environ. Health Perspect. 102 (1994) 3–5.
[38] J.C. McDonald, Epidemiological significance of mineral fiber persistence in human lung tissue, Environ. Health Perspect. 102 (1994) 221–224.
[39] R.F. Dodson, M.A.L. Atkinson, J.L. Levin, Asbestos fiber length as related to potential pathogenicity: a critical review, Am. J. Ind. Med. 44 (2003) 291–297.
[40] H. Nagai, S. Toyokuni, Biopersistent fiber-induced inflammation and carcinogenesis: lessons learned from asbestos toward safety of fibrous nanomaterials, Arch. Biochem. Biophys. 502 (2010) 1–7.
[41] A. Schinwald, T. Chernova, K. Donaldson, Use of silver nanowires to determine thresholds for fibre length-dependent pulmonary inflammation and inhibition of macrophage migration in vitro, Part. Fibre Toxicol. 9 (2012) 47.
[42] J.C. McDonald, B.G. Armstrong, C.W. Edwards, A.R. Gibbs, H.M. Lloyd, F.D. Pooley, D.J. Ross, R.M. Rudd, Case-referent survey of young adults with mesothelioma: I. Lung fibre analyses, Ann. Occup. Hyg. 45 (2001) 519–523.
[43] H. Nagai, Y. Okazaki, S.H. Chew, N. Misawa, Y. Yamashita, S. Akatsuka, T. Ishihara, K. Yamashita, Y. Yoshikawa, H. Yasui, L. Jiang, H. Ohara, T. Takahashi, G. Ichihara, K. Kostarelos, Y. Miyata, H. Shinohara, S. Toyokuni, Diameter and rigidity of multiwalled carbon nanotubes are critical factors in mesothelial injury and carcinogenesis, Proc. Natl. Acad. Sci. U. S. A. 108 (2011) 1330–1338.
[44] P.D. Ray, B.W. Huang, Y. Tsuji, Reactive oxygen species (ROS) homeostasis and redox regulation in cellular signaling, Cell. Signal. 24 (2012) 981–990.
[45] D.W. Kamp, S.A. Weitzman, The molecular basis of asbestos induced lung injury, Thorax 54 (1999) 638–652.
[46] B.T. Mossman, A. Churg, Mechanisms in the patheogenesis of asbestosis and silicosis, Am. J. Rep. 157 (1998) 1666–1689.
[47] C. Dostert, V. Pétrilli, R. Van Bruggen, C. Steele, B.T. Mossman, J. Tschopp, Innate immune activation through Nalp3 inflammasome sensing of asbestos and silica, Science 320 (80) (2008) 674–677.
[48] S.G. Rhee, H2O2, a necessary evil for cell signaling, science, 312 (80) (2006) 1882–1883.
[49] M.J. Morgan, Z. Liu, Crosstalk of reactive oxygen species and NF-κB signaling, Cell Res. 21 (2011) 103–115.
[50] A. Manke, L. Wang, Y. Rojanasakul, Mechanisms of nanoparticle-induced oxidative stress and toxicity, Biomed. Res. Int. 2013 (2013), 942916 (15 pages).
[51] C.S. Sharma, S. Sarkar, A. Periyakaruppan, J. Barr, K. Wise, R. Thomas, B.L. Wilson, G.T. Ramesn, Single-walled carbon nanotubes induces oxidative stress in rat lung epithelial cells, J. Nanosci. Nanotechnol. 7 (2007) 2466–2472.
[52] D.M. Brown, I.A. Kinloch, U. Bangert, A.H. Windle, D.M. Walter, G.S. Walker, C.A. Scotchford, K. Donaldson, V. Stone, An in vitro study of the potential of carbon nanotubes and nanofibres to induce inflammatory mediators and frustrated phagocytosis, Carbon N. Y. 45 (2007) 1743–1756.
[53] C.A. Dinarello, Interleukin-1, Cytokine Growth Factor Rev. 8 (1997) 253–265.
[54] Y.J. Arnoldussen, A. Skogstad, V. Skaug, M. Kasem, A. Haugen, N. Benker, S. Weinbruch, R.N. Apte, S. Zienolddiny, Involvement of IL-1 genes in the cellular responses to carbon nanotube exposure, Cytokine 73 (2015) 128–137.
[55] J. Dong, D.W. Porter, L.A. Batteli, M.G. Wolfarth, D.L. Richardson, Q. Ma, Pathologic and molecular profiling of rapid-onset fibrosis and inflammation induced by multi-walled carbon nanotubes, Arch. Toxicol. 89 (2015) 621–633.
[56] A. Fettelschoss, M. Kistowska, S. LeibundGut-Landmann, H.-D. Beer, P. Johansen, G. Senti, E. Contassot, M.F. Bachmann, L.E. French, A. Oxenius, T.M. Kündig, Inflammasome activation and IL-1β target IL-1α for secretion as opposed to surface expression, Proc. Natl. Acad. Sci. U. S. A. 108 (2011) 18055–18060.
[57] O. Gross, A.S. Yazdi, C.J. Thomas, M. Masin, L.X. Heinz, G. Guarda, M. Quadroni, S.K. Drexler, J. Tschopp, Inflammasome activators induce interleukin-1α secretion via distinct pathways with differential requirement for the protease function of Caspase-1, Immunity 36 (2012) 388–400.
[58] J. Palomäki, E. Välimäki, J. Sund, M. Vippola, P.A. Clausen, K.A. Jensen, K. Savolainen, S. Matikainen, H. Alenius, Long, needle-like carbon nanotubes and asbestos activate the NLRP3 inflammasome through a similar mechanism, ACS Nano 5 (2011) 6861–6870.
[59] J.M. Hillegass, J.M. Miller, M.B. MacPherson, C.M. Westbom, M. Sayan, J.K. Thompson, S.L. Macura, T.N. Perkins, S.L. Beuschel, V. Alexeeva, H.I. Pass, C. Steele, B.T. Mossman,

A. Shukla, Asbestos and erionite prime and activate the NLRP3 inflammasome that stimulates autocrine cytokine release in human mesothelial cells, Part. Fibre Toxicol. 10 (2013) 39.
[60] A.S. Yazdi, G. Guarda, N. Riteau, S.K. Drexler, A. Tardivel, I. Couillin, J. Tschopp, Nanoparticles activate the NLR pyrin domain containing 3 (Nlrp3) inflammasome and cause pulmonary inflammation through release of IL-1α and IL-1β, Proc. Natl. Acad. Sci. U. S. A. 107 (2010) 19449–19454.
[61] A. Schinwald, K. Donaldson, Use of back-scatter electron signals to visualise cell/nanowires interactions in vitro and in vivo; frustrated phagocytosis of long fibres in macrophages and compartmentalisation in mesothelial cells in vivo, Part. Fibre Toxicol. 9 (2012) 34.
[62] J.K. Lee, B.C. Sayers, K.-S. Chun, H.-C. Lao, J.K. Shipley-Phillips, J.C. Bonner, R. Langenbach, Multi-walled carbon nanotubes induce COX-2 and iNOS expression via MAP kinase-dependent and -independent mechanisms in mouse RAW264.7 macrophages, Part. Fibre Toxicol. 9 (2012) 14.
[63] D.W. Gilroy, P.R. Colville-Ash, D. Willis, J. Chivers, M.J. Paul-Clark, D.A. Willoughby, Inducible Cyclooxygenase may Have Anti-Inflammatory Properties, 5, 1999 10–13.
[64] B. Poligone, A.S. Baldwin, Positive and negative regulation of NF-kappaB by COX-2: roles of different prostaglandins, J. Biol. Chem. 276 (2001) 38658–38664.
[65] F. Krombach, S. Münzing, A.M. Allmeling, J.T. Gerlach, J. Behr, M. Dörger, Cell size of alveolar macrophages: an interspecies comparison, Environ. Health Perspect. 105 (1997) 1261–1263.